This document is downloaded from the
Digital Open Access Repository of VTT

Title	Solid oxide fuel cell stack temperature estimation with data-based modeling - Designed experiments and parameter identification
Author(s)	Pohjoranta, Antti; Halinen, Matias; Pennanen, Jari; Kiviaho, Jari
Citation	Journal of Power Sources. Elsevier. Vol. 277 (2015), Pages 464 - 473
Date	2015
URL	http://dx.doi.org/10.1016/j.jpowsour.2014.08.130
Rights	Post-print version of the article. This article may be downloaded for personal use only.

VTT
http://www.vtt.fi
P.O. box 1000
FI-02044 VTT
Finland

By using VTT Digital Open Access Repository you are bound by the following Terms & Conditions.

I have read and I understand the following statement:

This document is protected by copyright and other intellectual property rights, and duplication or sale of all or part of any of this document is not permitted, except duplication for research use or educational purposes in electronic or print form. You must obtain permission for any other use. Electronic or print copies may not be offered for sale.

Article manuscript accepted for publication in the Journal of Power Sources (2014-08-11)

Solid oxide fuel cell stack temperature estimation with data-based modeling – Designed experiments and parameter identification

Antti Pohjoranta*, Matias Halinen, Jari Pennanen, Jari Kiviaho

VTT Technical Research Centre of Finland, P.O. Box 1000, FI-02044, Finland

*Corresponding author: antti.pohjoranta@vtt.fi, tel. +358 40 570 9825

Abstract

Data-based modeling is utilized for the dynamic estimation of the temperature inside a solid oxide fuel cell (SOFC) stack. Experiment design and implementation, data pre-treatment, model parameter identification and application of the obtained model for the estimation and prediction of the SOFC stack maximum and minimum temperatures are covered. Experiments are carried out on a complete 10 kW SOFC system to obtain data for model development. An ARX-type (autoregressive with extra input) polynomial input-output model is identified from the data and Kalman filtering is utilized to obtain an accurate estimator for the internal stack temperatures. Prediction capabilities of the model are demonstrated and using the modeling approach for SOFC system monitoring is discussed.

Keywords

SOFC temperature estimation, ARX modeling, experiment design, Kalman filtering, solid oxide fuel cell

1 Introduction

Thermal management of solid oxide fuel cell (SOFC) stacks is essential for the successful deployment of SOFC based power systems. The general temperature level as well as the temperature distribution inside the SOFC stack affect both the stack performance and the rate of stack performance degradation [1, 2]. Therefore, it is fundamentally important to keep the stack temperature within a given range. To this end, it is necessary to have means for either measuring or estimating the temperature at various locations inside a SOFC stack. Installing temperature measurement devices directly in the stack is possible but adds to the system's complexity, thus increasing its price and decreasing its reliability. Estimating the stack temperature by using computational models leaves the system hardware intact but requires the effort of model development and deployment into system environment.

SOFC stack models based on physical first principles have proven very useful during the system design phase when an actual apparatus does not yet exist and the system operation must be studied over a wide, undefined operating envelope. However, as soon as the system is up and running it is often more efficient to create system-specific models based on measured system data. Data-based models, such as the polynomial input-output (I/O) models utilized in this work, are simple to identify and run, and their application-specific accuracy can surpass that of physics-based models. The main challenge in creating data-based models is in collecting representative data of the modelled process. The design of experiments methodology is useful in solving the conflict between data information content and cost of experimental effort. This paper documents the process of designing experiments for gathering data from a complete 10 kW SOFC system and using that data for model parameter identification and model validation. Finally, the identified model is utilized to estimate and predict the temperature inside the SOFC stack.

1.1 State of the art

The SOFC power system technology is still relatively young and presumably therefore the vast majority of SOFC models found in the literature are based on physical first principles. Numerous very advanced models have been published and extensive reviews of the SOFC modeling work based on 1st principles are found e.g. in [3-6]. The model outputs typically cover both the electrical variables (voltage, current, power) as well as the temperature (and the temperature distribution) within the SOFC. Fluid dynamics are also commonplace in physical SOFC models, which enables the analysis of flow and pressure fields in the modelled device. Often the computational requirement for solving 1st principle SOFC models is high, restricting the level of model detail. Therefore, the models often focus on, e.g., a single repeating unit within the SOFC stack instead the whole stack, or are reduced in physical dimensions (from three to 0-2 dimensions).

Purely data-based models (a.k.a. black box models) of SOFCs have also been developed [6, Sec. 5]. Most black box SOFC models published so far are based on some variant of so-called neural networks. Some recent developments also include Bayesian networks and statistical data analysis based on linear regression models [7-9]. An ARX-type (autoregressive with extra input) input/output polynomial model was used in [10] to implement the linear dynamic part in a Hammerstein-type SOFC model.

Black box models only simulate the outputs that were selected for modeling before data collection and the main restriction for black box model utilization stems from challenges with collecting proper data. Considering SOFC applications these challenges are mostly related to their very high operating temperature of ca. 600-900°C. Typical applications of reported black box SOFC models include the simulation of the electrical output of the SOFC stack and the temperature, and sometimes pressure, at the stack outlets which are easier to measure than e.g. stack outlet gas composition or internal stack temperature values. In some cases the data for model development is measured from a single cell or a short stack in a dedicated test rig, or even produced by a physical model, in order to reduce the required experimental effort [6]. While these special arrangements for data

acquisition are useful for the model development work, the so-obtained models are not directly applicable to complete SOFC stacks and systems.

The practical challenges related to the experimental work with SOFCs underline the importance of proper planning and execution of the data collection phase when developing black box SOFC models. The design of experiments methodology (DoE), covered in several textbooks such as [11], provides the analytical tools to optimize the amount of information that is obtained from the examined object with a given experimental effort. Within the field of fuel cell research, DoE has mainly been used for system behavior studies, especially in proton exchange membrane fuel cell (PEMFC) research [12-15]. In [9, 16, 17] DoE is utilized in particular for the analysis and the development of linear regression models of SOFCs.

1.2 Background and overview of this work

This work focuses on developing estimates of the stack temperature values inside a SOFC stack, by using linear dynamic, input/output (I/O) polynomial models whose parameters are identified from data. The aim of the work is to find such solutions that are practically feasible considering their implementation in embedded process control systems and their utilization for SOFC power system control.

The dependencies between internal SOFC stack temperatures and three system inputs, namely, load current, air flow and air temperature at stack module inlet, were experimentally evaluated in a preceding work [9, 18]. The experiments were carried out around a single specified nominal operating point and the models were created for the steady state estimation of the stack temperature by utilizing multivariable linear regression (MLR). All the evaluated inputs were found to have a significant effect on the stack temperature, and the stack cathode outlet temperature was found vitally important for accurate stack temperature estimation. Also, an MLR model was utilized for stack temperature regulation, and a preliminary study on I/O model identification was carried out in [19, 20].

In the current work, four system inputs are used in the experiments. These include the load current, air flow and air temperature at stack module inlet, as before, but also the system natural gas (NG) flow. The experiments were carried out in order to obtain such a series of data which enables creating models for the estimation of the stack temperature in both steady states as well as during transient operation over the whole relevant operating range (i.e. excluding start-up and shutdown). To meet these aims, the experiments were designed to fit within a pre-defined system operating space, and in particular, around two representative “central” operating conditions (Sec. 2). Thus, in comparison to the previous work [9, 18], the data series collected and used in this study is larger in terms of the number of inputs as well as their range of variation. In addition, the number of data points collected is larger than before, which enables splitting the data set to a part used for model development and another part used solely for model validation.

The gathered data is utilized to identify a polynomial I/O model with the ARX structure. This model structure has the advantages that (i) the parameters’ relationship to each input-to-output pair remains clear and (ii) the identification algorithm is very simple (Sec. 3.2). The obtained ARX model is re-cast to the state space format to enable simple utilization of the so-called Kalman filter [21] for the dynamic estimation of the temperatures (Sec. 3.4, 4.1). Finally, an optimal predictor for the stack temperature variables is built by utilizing the obtained estimate (Sec. 3.5, 4.2) and applying the modeling approach to SOFC degradation monitoring purposes is briefly discussed (Sec. 4.3).

2 Experimental

The experiments were carried out with a complete 10 kW SOFC system [22]. The system utilizes a single, planar, 80-cell SOFC stack produced by Versa Power Systems [23]. The stack is equipped with internal temperature measurement sensors. The system layout is illustrated in Figure 1.

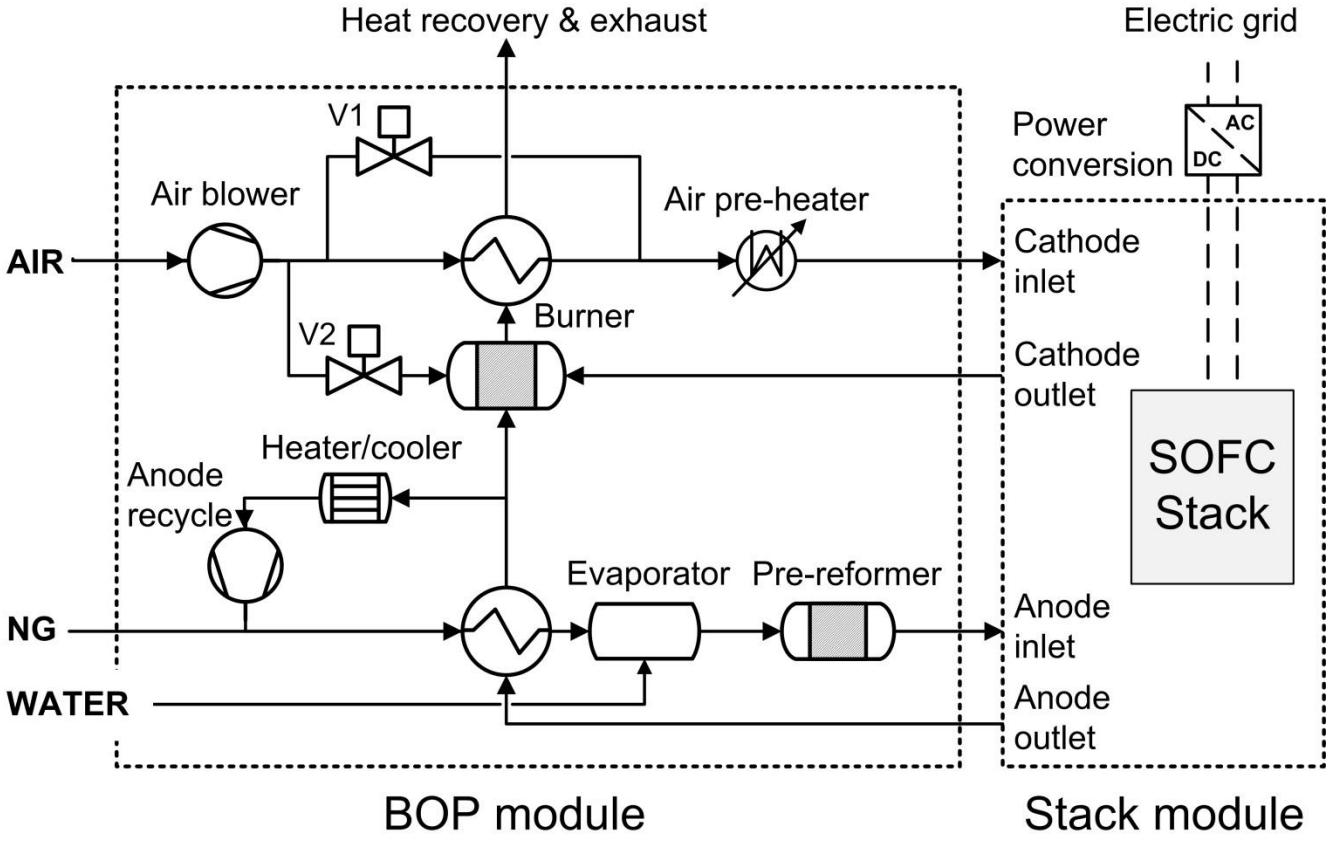

Figure 1 - Layout of the 10 kW SOFC system used in the experiments.

Load current (I, A), air flow ($\dot{V}_{air}$, dm^3 min^{-1}), air temperature at stack module inlet ($T_{air,in}$, °C) and system NG flow ($\dot{V}_{NG}$, dm^3 min^{-1}) were considered as independent system inputs in the experiment design (the volumetric flow being measured in 101325 Pa and 0°C). Stack maximum and minimum temperature (T_{max}, T_{min}, °C) and the cathode outlet temperature ($T_{cath,out}$, °C) were recorded as response. The stack maximum and minimum temperatures were determined by taking the maximum and minimum, respectively, of the values measured with 13 temperature measurement sensors installed inside the SOFC stack and distributed over one representative cell, located in the middle of the stack. Thus, in fact, they are the cell maximum and minimum temperature and together provide a representative value of the temperature difference over the cell. An additional 10 temperature measurement sensors were distributed over the stack to be certain that the temperature distribution in the direction of the stack height is sufficiently uniform. The cathode outlet temperature was measured from the cathode outlet flow, directly at the stack outlet.

No other control actions than those detailed in Sec. 2.1 were taken during the experiment run. The anode off-gas recycle flow rate was kept constant at 175 dm^3 min^{-1} throughout the experiment run and no particular action was taken to actively regulate the degree of pre-reforming or direct internal reforming of the fuel gas.

2.1 Experiment design

The experiment design used here extends that of the previous work [9], where it was found that while the three first inputs (I, $\dot{V}_{air}$ and $T_{air,in}$) as such have a statistically significant effect on the stack temperature, their interactions do not. This enabled omitting the interaction effects of these inputs from the current experimental design. Consequently, a so-called *fractional factorial design* (FFD) was obtained, and the assumption that the effect of the interactions between I, $\dot{V}_{air}$ and $T_{air,in}$ to the output is zero was utilized to reduce the number of experimental conditions in the design. Further details on experiment design and fractional factorial designs are found in [11].

The experimental domain is constrained by the limits of the feasible and safe operating range of the SOFC system. For instance, the load current and the air and NG flow must remain within a certain range in order to not deplete the cathode or anode of oxygen or fuel, respectively. Such constraints make it infeasible to fully randomize each independent input individually, as the resulting combination of inputs might be outside the operating boundaries. Therefore, the experiments were carried out in two parts, so that the relevant system operating space was sufficiently covered. In particular, the same fractional factorial design was carried out around two different central operating points. In both cases the variation of the inputs is the same and only the center point of the experiment domain changes. The complete experiment design is visually illustrated in Figure 2, and the input variables' variations as well as the two center points are given in

.

Table 1 - Experiment domain center points and inputs' variation.

Input	Unit	FFD1 center point	FFD2 center point	Variation
I	A	160	145	±5
$\dot{V}_{air}$	$dm^3\ min^{-1}$	1062	1023	±50
$T_{air,in}$	°C	735	745	±10
$\dot{V}_{NG}$	$dm^3\ min^{-1}$	27.90	25.77	±0.5

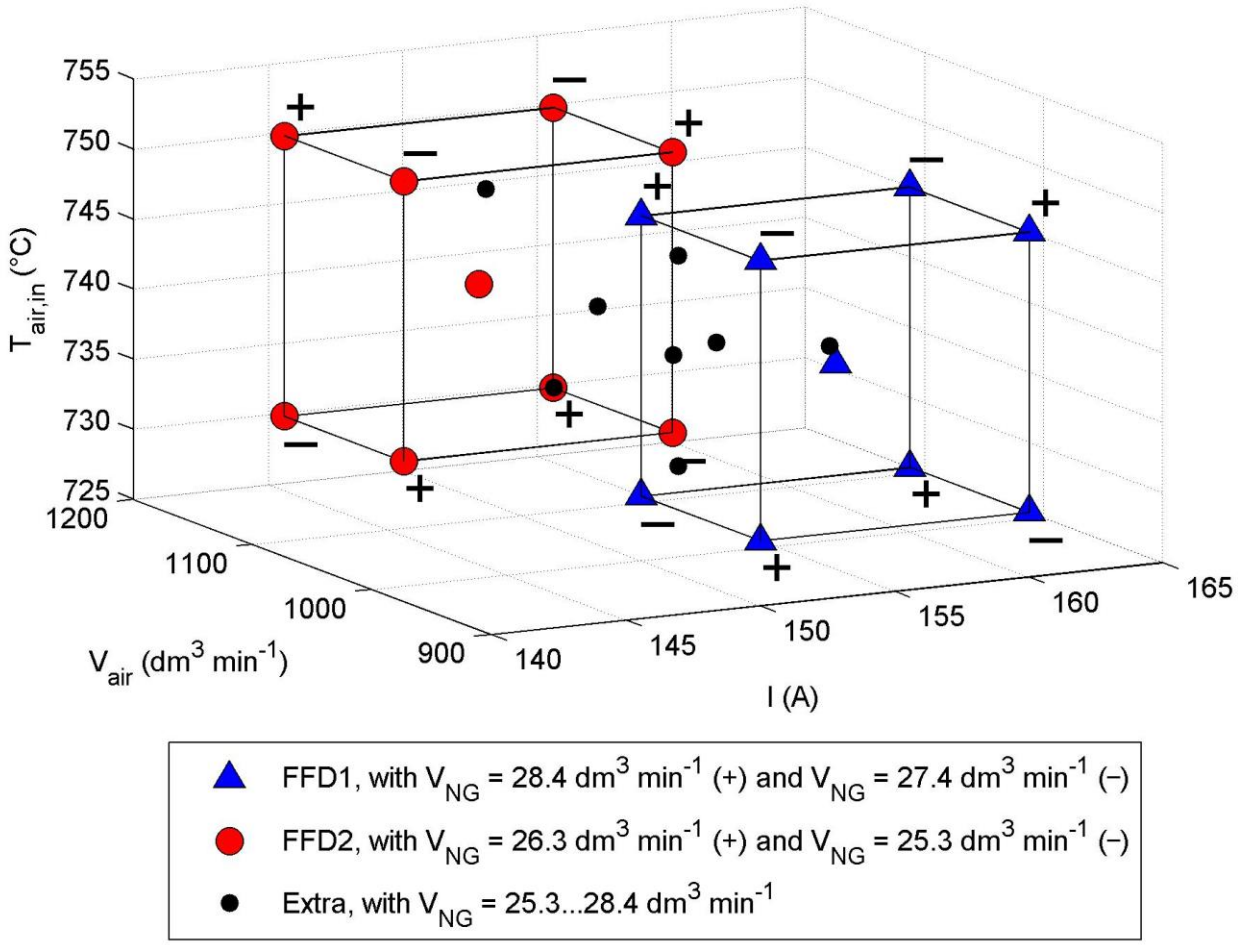

Figure 2 - Illustration of the experiment design and the covered system operating space. The two FFDs (and their center-of-domain points) are denoted by blue triangles and red circles. The measured extra data points are denoted by black dots. The natural gas flow per FFD point is indicated by the + and – signs.

In Figure 2, the cubes represent the fractional factorial experiments (FFD1 and FFD2) consisting of 8 experimental points around the experiment domain center points. The dots in Figure 2 are additional experimental points recorded to better cover the operating space and for model validation purposes. The + and – signs denote the value of $\dot{V}_{NG}$ at the FFD points. Note also that the central operating point of FFD1 is also the system design point ("nominal operating condition" or NOC).

The FFD structure was decided upon earlier experimental results [9]. Both FFDs are 2^{4-1} fractional factorial designs obtained with the design generator $\dot{V}_{NG} = I \cdot \dot{V}_{ir} \cdot T_{air,in}$ (with the defining relation $1 = I \cdot \dot{V}_{air} \cdot T_{air,in} \cdot \dot{V}_{NG}$). Therefore, the interactions between the inputs I, $\dot{V}_{air}$ and $T_{air,in}$ are aliased with (i.e. cannot be distinguished from) the interactions between these inputs and the fourth input $\dot{V}_{NG}$. (Specifically, the undistinguishable interaction pairs are (i) $I \cdot \dot{V}_{air}$ and $T_{air,in} \cdot \dot{V}_{NG}$, (ii) $I \cdot T_{air,in}$ and $\dot{V}_{air} \cdot \dot{V}_{NG}$ and (iii) $\dot{V}_{air} \cdot T_{air,in}$ and $I \cdot \dot{V}_{NG}$.) Additionally, all three-input interactions are aliased with the remaining single input (e.g. the effect of I is aliased with the interaction effect of $\dot{V}_{air} \cdot T_{air,in} \cdot \dot{V}_{NG}$) and so also the three-input interactions are all assumed zero. However, the chosen FFD does enable identifying the effects of the two-input interactions,

where $\dot{V}_{NG}$ is one factor (presuming the effect of the other two-input interactions is negligible). Therefore, compared to earlier experiments, the potentially interesting new interaction effects are covered by the experiment design.

The input data time-series are shown in Figure 3. The experimental points of each FFD were completed in a randomized order and each operating condition was held constant for ca. 24 hours so that the system had time to stabilize. The system was set to its nominal condition for the weekends in order to record reference data for monitoring any changes that might occur in system performance, such as stack voltage degradation. The system's response (T_{max}, T_{min} and $T_{cath,out}$) corresponding to the input data is shown in Figure 4.

For modeling purposes, the collected full data set is divided into one part that is utilized for model parameter identification ("identification data") and another part which is used for model validation and performance evaluation ("validation data"). The data segments used for model identification and validation are also denoted in Figure 3 and Figure 4. (Some data is left unused in this work to enable a better resolution in the result figures. This does not essentially affect the results.)

Two criteria were considered important when dividing the data set; (i) the identification data should sufficiently well span the whole operating domain of the system and (ii) the validation data should include several such operating conditions which are not exactly included in the identification data. To fulfill the first criterion, the identification data set is extended to cover also early parts of FFD2 and so the large variations in the load current, taking place during the FFD2 experiments, are included in the identification data. Secondly, although the FFD2 conditions are all different to the FFD1 conditions, several extra data points, where the operating conditions were determined randomly, within the given operating domain, were measured and included in the validation data.

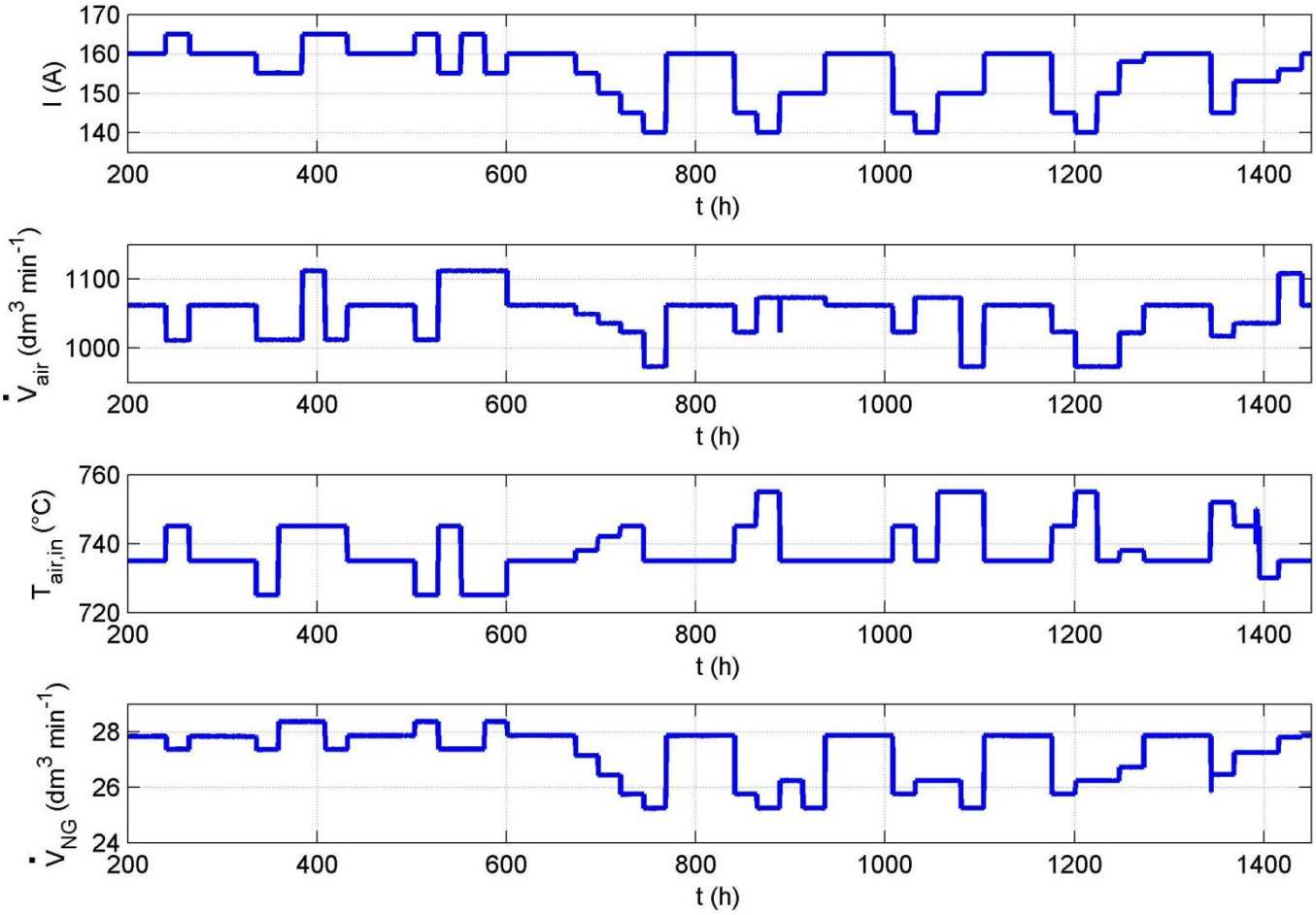

Figure 3 - System inputs during the experiment.

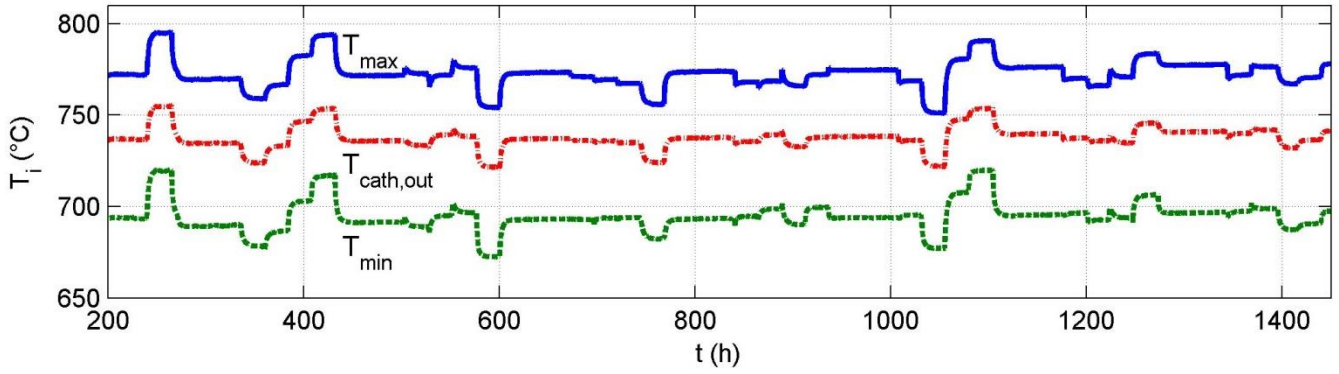

Figure 4 - System response during the experiment.

3 Modeling and estimation

The modeling process consists of data pretreatment and model identification, i.e. the selection of a suitable model structure and the calculation of its parameters based on the pretreated data.

3.1 Data pretreatment

The measured input/output (I/O) data was pretreated by down-sampling and by removing the nominal operating condition from the data. The pretreated I/O data variables are denoted by $u_{1\ldots4}$ and $y_{1\ldots3}$, corresponding to the inputs I, $\dot{V}_{air}$, $T_{air,in}$ and $\dot{V}_{NG}$, and the outputs T_{max}, T_{min} and $T_{cath,out}$, respectively. Figure 5 displays the pretreated output data $y_{1\ldots3}$ during the test run.

Down-sampling of the data was done as the measurement data was originally recorded with a sampling rate of one sample per second (1 Hz). The original sampling rate is excessively high for model parameter identification in the case at hand since the time constants of the thermal phenomena in the system are in the order of hours. Therefore, the measurement data was down-sampled to a sample rate of one sample per five minutes (1/300 Hz).

In order to maintain consistency between the dynamic and static behavior of the identified model, the nominal operating condition (NOC) value is removed from the data ("offset removal", [24, Ch. 14]). The NOC value for the outputs was that obtained at200 hours from the start of the experiments. The values for the NOC are given in Table 2. Removing the NOC value effectively transforms the measurement data into data which describes the system deviation from the said nominal operating condition. Figure 5 illustrates that the outputs' deviation is between ±30°C from the NOC during the experiment. The removed nominal values, listed in Table 2, are stored for eventually returning the estimated output values to the actual operating output value.

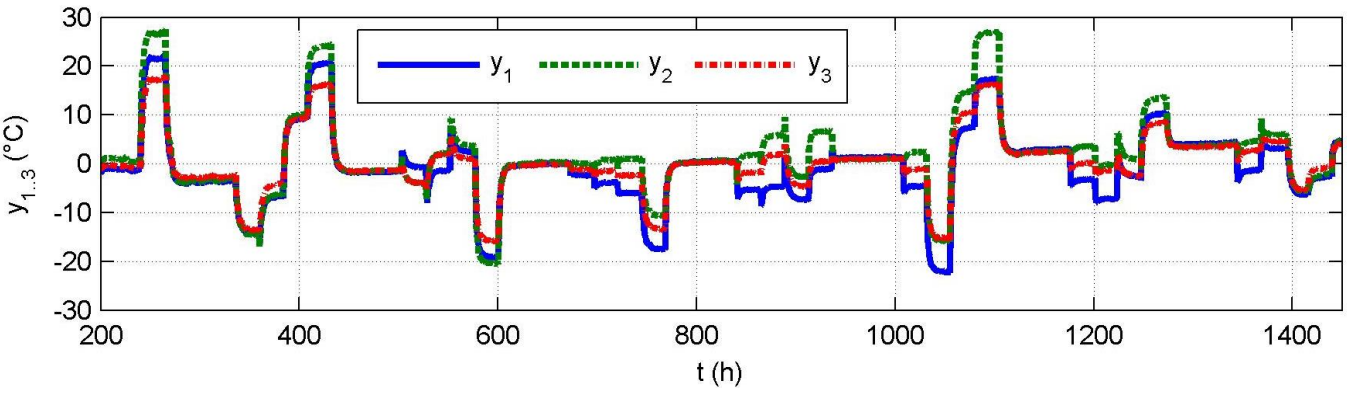

Figure 5 - The pretreated output data.

Table 2 - Nominal operating conditions removed from measurement data during data pre-treatment.

	NOC value	Unit	Symbol
Inputs			
I	160.0	A	u_1
$\dot{V}_{air}$	1062	$dm^3\ min^{-1}$	u_2
$T_{air,in}$	735.0	°C	u_3
$\dot{V}_{NG}$	27.90	$dm^3\ min^{-1}$	u_4
Outputs			
T_{max}	773.3	°C	y_1
T_{min}	692.9	°C	y_2
$T_{cath,out}$	737.3	°C	y_3

3.2 Model identification

The pretreated data was used to identify a discrete-time, multiple-input, multiple-output (MIMO) model with the ARX structure (1).

$$y(t) + A_1 y(t-1) + \cdots + A_{n_a} y(t-n_a) = B_0 u(t-n_k) + B_1 u(t-n_k-1) + \cdots + B_{n_b} u(t-n_k-n_b) + e(t) \quad (1)$$

Equation (1) is more compactly expressed as (2).

$$\sum_{i=0}^{n_a} A_i\, y(t-i) = \sum_{i=0}^{n_b} B_i\, u(t-n_k-i) + e(t) \quad (2)$$

In (1)-(2), $t = 0,1,2$ ... denotes the discrete time index of the data rather than the continuous time value. A_i and B_i are the model parameter matrices with dimensions $n \times n$ and $n \times m$, where $n > 1$ and $m > 1$ correspond to the number of outputs and inputs, respectively. $A_0 = I_{n\times n}$ and if there is a dead time of n_k samples in the process during which the response does not change after an input variation, then $B_{0\ldots n_k-1} = 0_{n\times m}$. (This corresponds to shifting the input data forward by n_k samples.)

The data vectors $y(t)$ and $u(t)$ contain the individual (pretreated) outputs and inputs, i.e., $y(t) = [y_1(t) \quad \cdots \quad y_n(t)]^T$ and $u(t) = [u_1(t) \quad \cdots \quad u_m(t)]^T$. $e(t)$ is a vector of model errors $(n \times n)$.

The parameters n_a and n_b denote the model order and define how many lagged outputs and inputs, respectively, are considered in the model.

For parameter calculation purposes, the parameters are collected into the $n \cdot n_a + m \cdot n_b \times n$ matrix $\theta = [A_1 \quad ... \quad A_{n_a} \quad B_1 \quad ... \quad B_{n_b}]^T$.

Correspondingly, the data for parameter calculation is collected to the $n \cdot n_a + m \cdot n_b$ –dimensional column vector $\varphi(t) = [-y^T(t-1) \quad ... \quad -y^T(t-n_a) \quad u^T(t-1) \quad ... \quad u^T(t-n_b)]^T$. By this arrangement, the optimal estimate for the parameters is found with (3), which implements the well-known least squared errors parameter identification strategy.

$$\hat{\theta} = \left[\frac{1}{N}\sum_{t=1}^{N} \varphi^T(t)\varphi(t)\right]^{-1} \frac{1}{N}\sum_{t=1}^{N} \varphi(t)y^T(t) \qquad (3)$$

In (3) N denotes the number of samples used for parameter estimation.

For derivation, proofs and further details on the parameter calculation procedure and system identification in general see e.g. [24].

3.3 Simulation

The simulated output $\hat{y}^{sim}$ of the identified model is obtained simply as (4).

$$\hat{y}^{sim}(t) = -\sum_{i=1}^{n_a} A_i\, \hat{y}^{sim}(t-i) + \sum_{i=0}^{n_b} B_i\, u(t-i) \qquad (4)$$

In (4), the measured outputs y are simply replaced by the corresponding simulated values. As the first parameter matrix in A is the identity matrix ($A_0 = I_{n\times n}$) the present value of the simulated output $\hat{y}^{sim}(t)$ is obtained simply by subtracting the lagged simulated outputs ($\hat{y}^{sim}(t-k)$, $k > 0$) weighted by A_i from the right-hand-side of (2). The system input $u(t)$, which is defined by the operator, is the only input to the model.

3.4 Output estimation with Kalman filtering

The simulated output obtained with (4) is often inaccurate, especially when operating far from the nominal operating point (or the center point of the identification data in general). The accuracy of the calculated output can, however, be improved by utilizing the available measurements. In the case at hand, the internal stack temperatures ($\boldsymbol{T_{max}}$, $\boldsymbol{T_{min}}$) are presumed to be non-measureable in a real SOFC power system, but with the data measured at the lab, we have identified a model, (1), that produces estimates of both the internal stack temperatures as well as the stack cathode outlet temperature ($\boldsymbol{T_{cath,out}}$), which is considered always

measureable. Based on previous work [9, 18] and by observing the output plots in

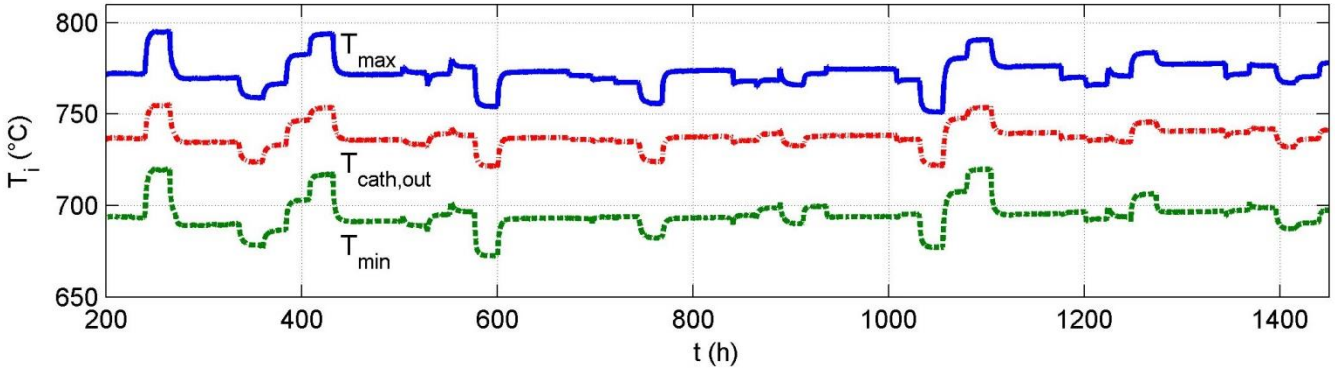

Figure 4-Figure 5, it is clear that all three output temperatures are significantly correlated, which is natural, considering that they are all measured from the same physical object. This correlation can be utilized to obtain information of the non-measureable variables through the measureable ones by using the identified model and the *Kalman filter* [24, 25].

The Kalman filter is a series of equations which provide an optimal (in the sense of minimal estimation error variance) way to combine measurement information with the information provided by a model. In our case, the filter is applied to improve the accuracy of the modelled output for T_{max} and T_{min} by utilizing the information obtained from the $T_{cath,out}$ measurement. The so obtained filtered output is here denoted the *estimate* of T_{max} and T_{min}.

Applying the filter is straightforward when a model that is in the state-space form can be used. The ARX-type, MIMO, polynomial model (1) is transformed into the discrete-time state-space format (5) by re-arranging the parameter matrices as shown in (6).

$$x(t) = Fx(t-1) + Gu(t-1) + w(t-1)$$
$$y(t) = Hx(t) + v(t) \qquad (5)$$

The model inputs and outputs remain the same, u and y, respectively, and x is the state vector with dimension $p = n_a \cdot n + (n_b + n_k - 1) \cdot m$. The F, G and H matrices (with dimensions $p \times p$, $p \times m$ and $n \times p$, respectively) are the state-space model parameter matrices, obtained from A and B as given in (6).

$$F = \begin{bmatrix} -A_1 & \cdots & -A_{n_a} & B_1 & \cdots & B_{n_b} \\ \hline I_{(n_a-1)\cdot n \times (n_a-1)\cdot n} & & 0_{(n_a-1)\cdot n \times n} & & 0_{(n_a-1)\cdot n \times (n_b+n_k-1)\cdot m} & \\ \hline 0_{(n_b+n_k-1)\cdot m \times n_a \cdot n} & & 0_{m \times (n_b+n_k-2)\cdot m} & I_{(n_b+n_k-2)\cdot m \times (n_b+n_k-2)\cdot m} & 0_{m \times m} & 0_{(n_b+n_k-2)\cdot m \times m} \end{bmatrix}$$

$$G = \begin{bmatrix} 0_{n_a \cdot n \times m} \\ I_{m \times m} \\ 0_{(n_b+n_k-2)\cdot m \times m} \end{bmatrix} \qquad H = [-A_1 \quad \cdots \quad -A_{n_a} \quad B_1 \quad \cdots \quad B_{n_b}] \qquad (6)$$

As the state-space representation is obtained from the identified ARX-model, the states $x_{1\ldots p}$ correspond to the lagged system outputs and inputs included in the ARX-structure. The ones and zeros in the F matrix are filled-in to appropriately shift back in time the terms stored in the state vector.

The terms w and v in (5) denote modeling and measurement error, respectively, which are assumed white, zero-mean, uncorrelated noise signals with known covariance matrices, Q and R, respectively. Often values for both of these have to be assumed by the user. However, the measurement error variance can also be obtained directly from the equipment specifications and if the states are known, or can be uniquely computed from data, then the modeling error covariance can also be estimated from data.

The state-space formulation given in (5) assumes that the process dead time is at least one sample time (i.e. in the ARX model $n_k \geq 1$). In case no dead time exists ($n_k = 0$), then the corresponding direct effect term is added on the second line of (5).

Remark – There are also well-established algorithms for identifying models with the state-space structure directly from data, but these are considerably more complicated than the least squared errors algorithm used for the ARX parameter calculation. Furthermore, when a state-space system is identified directly from data, the physical content of the states is easily left unexplained.

3.4.1 Obtaining the Kalman filter and the filtered output

For simplicity, the Kalman filter considered in our case is the steady-state discrete-time form of the filter (without extensions to cover system nonlinearities or time-variance). The filtered system output estimate $\hat{y}^+$ at each time instant is computed as

	$\hat{y}^+(t) = H\hat{x}^+(t)$	(7)

where the filtered state estimate $\hat{x}^+$ is obtained as shown in (8).

	$\hat{x}^-(t) = F\hat{x}^+(t-1) + Gu(t-1)$ $\hat{x}^+(t) = \hat{x}^-(t) + K\big(y(t) - H\hat{x}^-(t)\big)$	(8)

It is seen that the filtered state estimate $\hat{x}^+$ (a.k.a. updated state estimate) is a weighed sum of the unfiltered state-estimate $\hat{x}^-$ (obtained with the model and based on previous data) and the unfiltered estimate error $y(t) - H\hat{x}^-(t)$ (obtained based on the available measurements y).

The weighting factor K, called the Kalman gain, is obtained in our case by iterating the equation system (9) until stable values for K and P are obtained. P is the covariance of the estimation error and i is the iteration index.

	$P^-(i) = FP^+(i-1)F^T + Q$ $K(i) = P^-(i)H^T(HP^-(i)H^T + R)^{-1}$ $P^+(i) = (I - K(i)H)P^-(i)(I - K(i)H)^T + K(i)RK^T(i)$	(9)

Remark – As is seen in (9), K and P do not depend on the measured data, but only on the system model (F and H), the model error covariance (Q) and the measurement noise covariance (R). As our model and the errors are assumed time-invariant, the Kalman filter gain K can be computed offline, prior to implementation.

Finally, it is necessary to clarify that not all of the measurements, which were available during model identification, are considered to be available when the Kalman filter is actually operated. Therefore, when computing the filtered state estimate $\hat{x}^+$, the measurement vector y is completed with zeros on behalf of the not-measured outputs during operation. In our case, only the cathode outlet temperature is directly measured and so $y(t) = [0 \quad 0 \quad y_3(t)]^T$. The state-space representation and the Kalman filter structure take care of distributing the real measurement information between the filtered (or updated) estimates appropriately.

3.5 Output prediction

The simulated output, obtained with (4), is based *only* on the system inputs u set by the operator. Such an output may be computed as far to the future as the system inputs are known. The filtered estimate, obtained with (1) and (5)-(9), on the other hand, relies on the up-to-date value of the cathode outlet temperature measurement and can thus be obtained only at the present time instant, even if the operator inputs in the future were known. Compared to the simulation, however, the estimate is significantly more accurate. In order to improve the accuracy of the predicted system output, these two mechanisms can be combined, so to utilize all the available measurement data *and* the known operator inputs in parallel. Such a *k-step-ahead prediction* of the system output is obtained with (10).

	$\hat{y}(t\|t-k) = \bar{A}_k(q)B(q)u(t) + [1 - \bar{A}_k(q)A(q)]y(t)$	(10)

In (10), k is the number of sample times for which the system output is predicted. The notation $\hat{y}(t|t-k)$ underlines that in order to obtain $\hat{y}$ (i.e. the output estimate) at time index t, only the information of y up to time index $t-k$ is utilized.

$A(q) = 1 + A_1 q^{-1} + \cdots + A_{n_a} q^{-n_a}$, $B(q) = B_0 + B_1 q^{-1} + \cdots + B_{n_b} q^{-n_b}$ and $\bar{A}_k(q)$ are polynomials in q, which is the forward shift operator (i.e. $qu(t) = u(t+1)$ and $q^{-i}u(t) = u(t-i)$). The coefficients for $\bar{A}_k(q)$are given by (11)

	$\bar{A}_k(q) = \sum_{i=0}^{k-1} \tilde{A}_i \, q^{-i}$	(11)

where $\tilde{A}_i$ are the coefficients of $A^{-1}(q)$ (the inverse of $A(q)$). Only the k first elements $\tilde{A}_{0\ldots k}$ are required for the k-step-ahead prediction and these are found recursively by using the condition (12).

	$\sum_{i=0}^{l} \tilde{A}_i A_{l-i} = \begin{cases} I, & \text{if } l = 0 \\ 0, & \text{if } l \neq 0 \end{cases}, \qquad l = 0,1,\ldots,k$	(12)

To summarize, in (10), the input u, the model (A and B) as well as the available measurements y are utilized to obtain a prediction of the system output. In our case, however, the system output is not fully available as T_{max} and T_{min} cannot be directly measured, and therefore the estimated output $\hat{y}^+$ is used instead. The coefficients $\bar{A}_k(q)$ can be calculated offline and only the explicit output prediction calculation needs to be carried out online at each time step, as new measurement data from the system is obtained.

4 Results and discussion

4.1 Simulation and estimation

By using the identification data, an ARX model (1) with four inputs ($u_{1\ldots4}$, $m = 4$) and three outputs ($y_{1\ldots3}$, $n = 3$) was identified with the model orders $n_a = n_b = 3$ and dead time $n_k = 1$. These model parameter values were selected as a compromise between model accuracy and complexity, and are based on trial and error over the range 0…6 for n_a and n_b and 0…6 for n_k. Different orders for the different inputs or outputs were not considered.

The simulated model output, obtained with (4), for the stack T_{max} and T_{min} over the validation data is shown in Figure 6(a)-(b) by the green dashed lines. The corresponding estimate errors are shown in Figure 6(c)-(d). (The cathode outlet temperature data is not shown for brevity.)

The output estimate of the stack T_{max} and T_{min} obtained by using the identified model, (1), and a Kalman filter calculated based on the model, (5)-(9), is shown in Figure 6(a)-(b) by the red dash-dot line. The corresponding estimate errors are also shown in Figure 6(c)-(d).

The noise covariance parameters $R = I_{n\times n}$ and $Q = I_{p\times p}$ were used for computing the gain K. (Here $p = 21$, is the number of states in the state-space representation (5) of the model.) Furthermore, as two of the outputs ($y_1(t)$ and $y_2(t)$) are considered not measured, the two first rows of H were set equal to zero for calculating K (i.e. when iterating (9)). For the estimate calculation purposes, H is returned to its identified value.

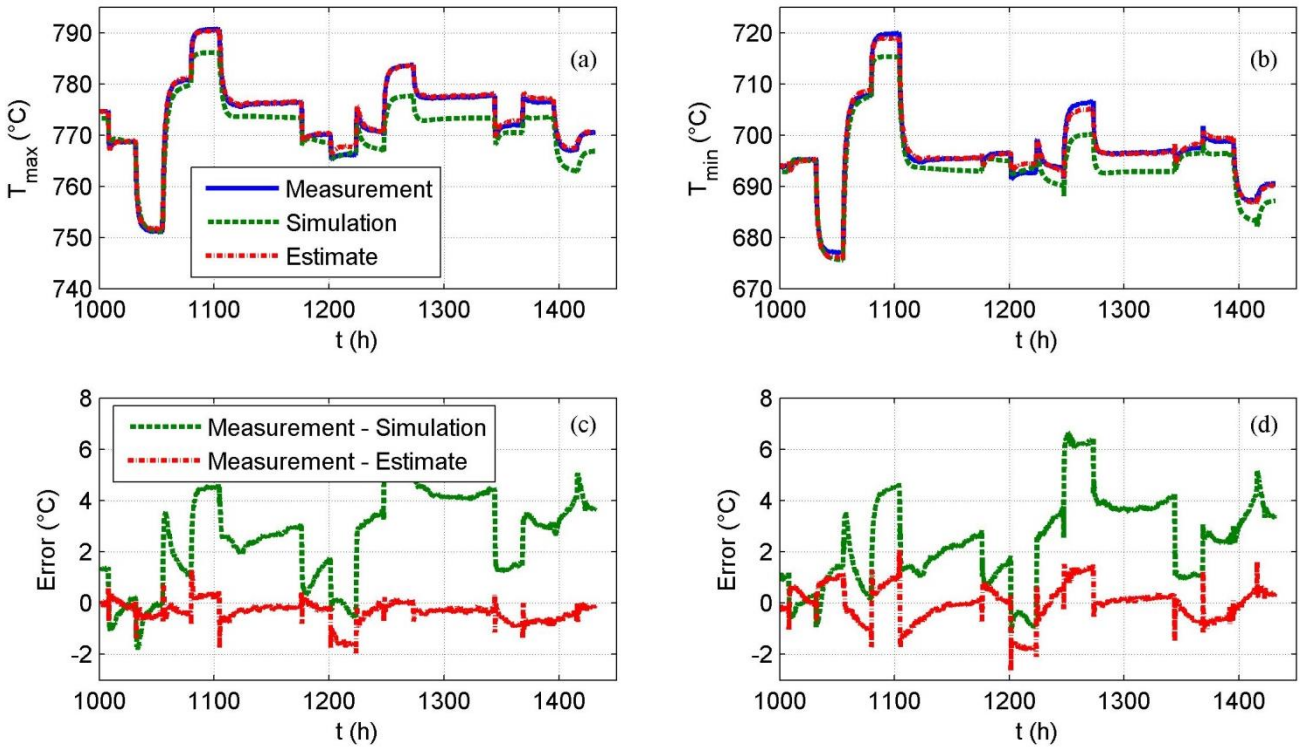

Figure 6 - The measured, simulated and estimated stack maximum and minimum temperature (a)-(b) and the corresponding errors (c)-(d) over the validation data set.

In Figure 6 the estimate for T_{max} and T_{min} obtained by using the Kalman filter is significantly more accurate than the simulated output. In particular, the simulated output is consistently smaller than the measured output value, indicating that the rising trend in the temperatures due to stack degradation is not fully captured. The error of the filtered estimate is within 1°C in the validation data for most of the time, also during transients and despite the degradation trend present in the data. Therefore, the estimate may be considered reliable and its utilization for output prediction purposes may be considered.

4.2 Prediction

A k-step-ahead prediction for T_{max} and T_{min} is calculated by using the model, (1), and the predictor obtained with (10)-(12) .

Figure 7 (a)-(b) displays the stack maximum and minimum temperatures predicted over a fixed six-hour interval (k = 72) over the validation data set. The corresponding simulated output temperatures and the measurements are also shown for comparison. The prediction is notably more accurate than the pure simulation, as can be seen also by comparing the error signals in Figure 7 (c)-(d). The error remains mostly within 2°C for the six-hour prediction, which is more than sufficient for, for example, model predictive control purposes.

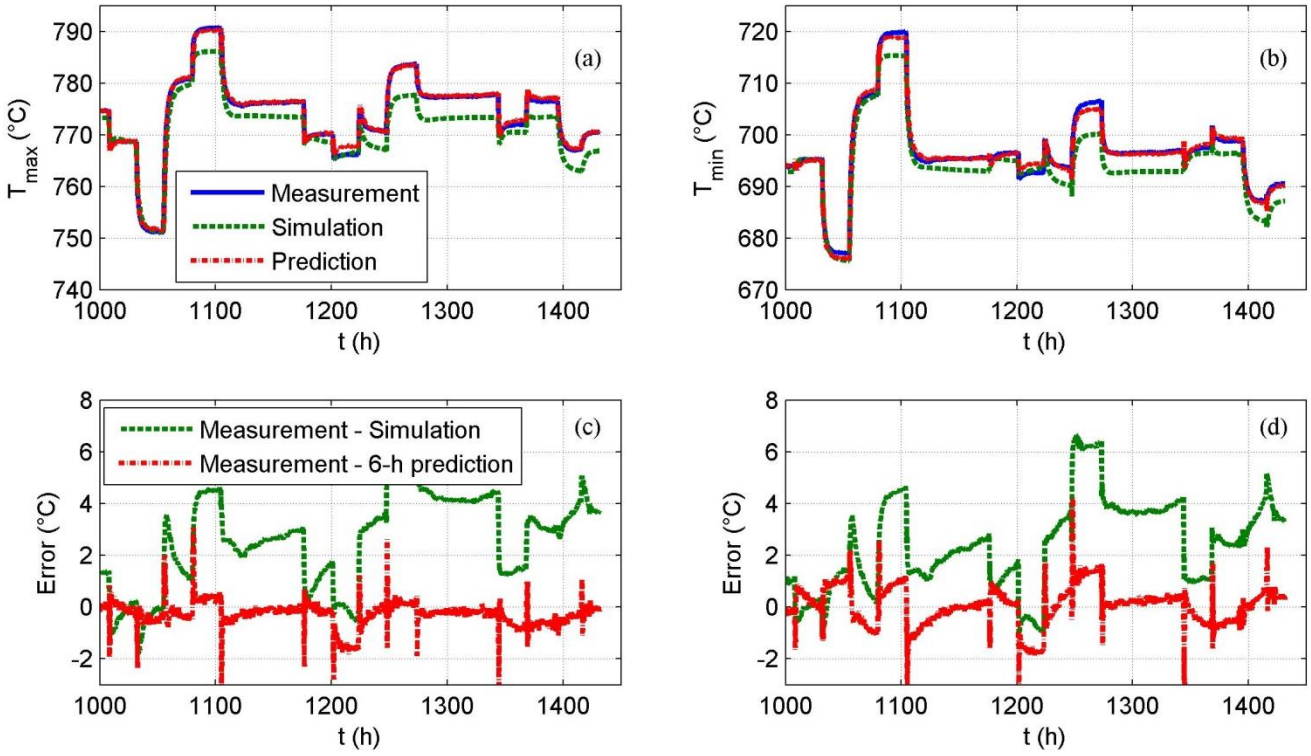

Figure 7 - The stack maximum and minimum temperature predicted six hours forward and compared with the measured value and the simulation (a)-(b) over the validation data set. The corresponding errors are shown in subfigures (c)-(d).

To further evaluate the prediction accuracy and the prediction behaviour in time, the predicted maximum stack temperature over fixed time intervals of 1, 6, 12 and 24 hours are shown in Figure 8. It is seen that the prediction accuracy improves as the prediction interval becomes shorter (and the prediction approaches the measured

value). Correspondingly, when the prediction interval is long, the prediction approaches the simulated value. This highlights the main difference between the predicted output and the simulated output – the prediction corrects itself as more information of the system is obtained with time.

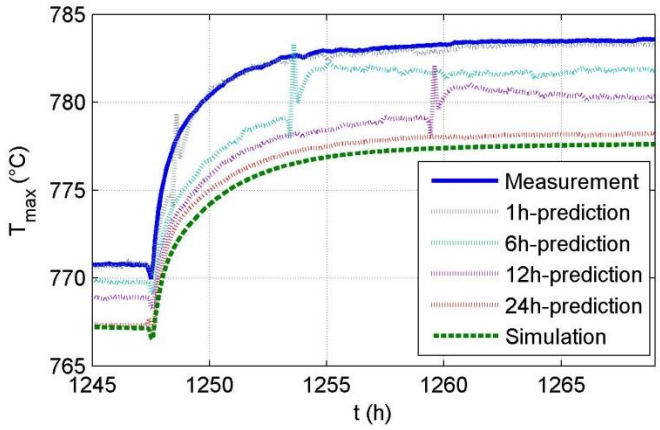

Figure 8 - The stack maximum temperature predicted over the fixed prediction intervals of 1, 6, 12 and 24 hours, compared with the measured and simulated temperature.

4.3 Considerations on model identification for system diagnosis, control and estimation purposes

For system diagnostics it would be useful to have a means to distinguish which changes in the system are due to normal wear and aging, and which might be caused by an incipient or evolving fault. For fuel cell systems in particular, the stack performance degradation is a phenomenon, which affects the whole system and should be monitored somehow. The performance degradation of the stack can be observed in the system outputs, in particular, in the stack temperature as well as the stack voltage (not shown here). In our case, the raising trend of ca. 5-7 °C / 1000 hours of operation in the stack temperature is due to performance degradation. However, to quantify what part of the stack temperature change is due to degradation and what is due to the operating conditions, the system must always be brought to a chosen reference state (in our case, the nominal operating conditions). By doing so, the stack temperature now and in the beginning of stack life can be clearly compared.

It is proposed, that with the data available from a system it is possible to identify a model which can be used to estimate the *nominal* behavior of the system – as if no degradation was present. If there is no degradation present in the original measurement data, then a model whose parameters are obtained by direct identification from the data, as done in Section 4.1, is automatically such a model. However, if the degradation effects are already present in the identification data, then the identification data should be further pre-treated simply by removing the degradation effects from the measured data, i.e. by removing the rising trend in the output data used for model identification. The obtained model, denoted the *nominal system model*, can then be used to evaluate how strong the degradation is, also in other operating conditions than the reference state.

Figure 9 displays the simulated stack maximum temperature obtained by simulating the nominal system model (which is obtained after de-trending the identification data) over the validation data period. The same procedure and the same model orders were used for identifying the nominal model as were used in Sections 3.2 and 4.1, respectively. The measurement and the ~~estimate~~ simulated output obtained in Section 4.1, and the de-trended output data, are shown for comparison. It is seen, that neither the nominal model nor the simulated output from Section 4.1 ~~does not~~ follow the rising trend in the temperature value, but instead, underestimate~~s~~ the stack maximum temperature continuously. The nominal model output is, however, on average closer to the de-trended

output than the original system model, the mean absolute errors being 1.3 °C and 1.7 °C, respectively (ca. 25% in favor to the nominal model). Both models are, however, inaccurate at some operating states, whereby the problem reverts back to the experiment design step. The difference between the simulated nominal temperature and the estimated temperature value may be considered as a quantitative measure for stack degradation during system operation.

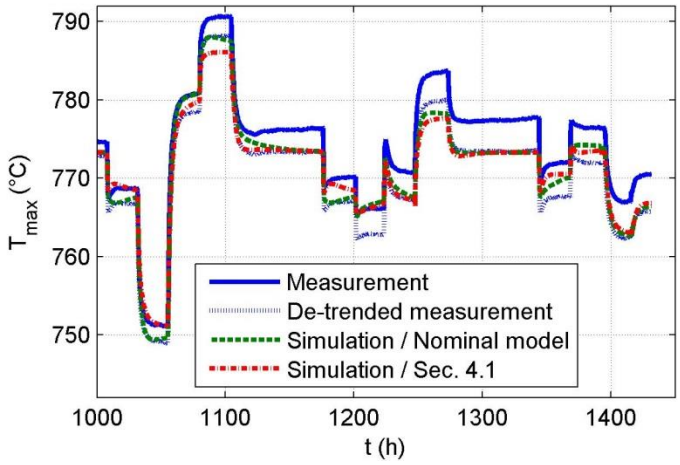

Figure 9 - Simulated stack maximum temperature obtained with the nominal system model.

The de-trending of output data is also useful when the model is identified for system control development purposes. In this case, however, data de-trending has a different function than above – now de-trending is carried out to highlight the process "short-term dynamics" (e.g. thermal transients) in the measurement data by removing the effects of "long-term dynamics" (i.e. degradation) before model identification. The increase in model transient operation accuracy may come at the expense of model steady-state accuracy, but steady-state accuracy can in the end be compensated for by feedback and an integrating action in the control.

Considering estimation, which is the original application presented here for the identified models, removing the degradation trend from the measured output data was found harmful. This pre-treatment not only decreases the model accuracy (with respect to the degrading process) but also removes all useful correlation between the measured cathode outlet temperature and the not-measured stack internal temperatures, thus deteriorating the estimation accuracy even after application of the Kalman filter.

4.4 A note on data-based models

It should be emphasized that the approach presented here is entirely reliant on the underlying measurement data. While the approach has several merits such as simplicity and case-wise accuracy, the downside with a data-based approach is that the computational system can replicate only those phenomena that are present in the identification data. Therefore the effects of, for example, local fractures in the SOFC stack seals or the SOFC ceramic layer, which cause leakages and subsequent local hot-spots much hotter than the measured maximum temperature, cannot be estimated or predicted by the models presented here. The same applies to changes – intentional or unexpected – in such system inputs which were kept constant during collection of the identification data. These are features common to all data-based approaches and must be born in mind when

designing the experimental arrangement intended for data collection. With physics-based models, the case is analogous regarding phenomena whose equations are not included in the model.

5 Conclusions

This paper documents a complete process carried out to create and utilize dynamic models for SOFC stack temperature estimation. The work starts from data acquisition with designed experiments then proceeding to model identification and validation, as well as application of the model for system output estimation and prediction.

An extended series of designed experiments was carried out on a complete 10 kW SOFC system. The experiment design consisted of two 2^{4-1} fractional factorial experiments, carried out around two different experiment domain center points. Four independent inputs (current, air flow, air temperature at stack module inlet and natural gas flow) were adjusted and the stack minimum, stack maximum and cathode outlet temperatures were measured as response.

Parameter identification of an ARX-type MIMO model for the said temperatures was carried out and the obtained model was applied with Kalman filtering to obtain highly accurate estimates of the stack temperature variables. Good prediction capabilities of the obtained model were demonstrated over prediction intervals of 1-24 hours.

All the developed models and filters are linear and time-invariant, discrete-time systems, meaning that their utilization in an embedded system environment can be done with standard equipment and no iterative solver algorithms are necessary.

Acknowledgements

This work was carried out as a part of the RealDemo project which was funded by the Finnish Funding Agency for Innovation (Tekes), VTT and participatin industrial companies. Their financial support is gratefully acknowledged. The authors also thank all the numerous people who helped in carrying out the experiments discussed in this paper.

Glossary

ARX	Autoregressive (model) with extra input
DoE	Design of experiments (methodology)
FFD	Fractional factorial (experiment) design
I/O	Input-output
MIMO	Multiple-input-multiple-output
NG	Natural gas
NOC	Nominal operating conditions

PEMFC	Proton exchange membrane fuel cell
SOFC	Solid oxide fuel cell

References

[1] R. Knibbe, A. Hauch, J. Hjelm, S. Ebbesen and M. Mogensen, Durability of Solid Oxide Cells, *Green*, **1**, 141-169, 2011

[2] A. Nakajo, Z. Wuillemin, J. Van herle and D. Favrat, Simulation of thermal stresses in anode-supported solid oxide fuel cells stacks. Part I: Probability of failure of the cells, *J. Power Sources*, **193**, 203-215, 2009

[3] S. Kakaç, A. Pramuanjaroenkij, X.Y. Zhou, A review of numerical modeling of solid oxide fuel cells, *Int. J. Hydrogen Energy*, **32**, 761-786, 2007

[4] C.O. Colpan, I. Dincer and F. Hamdullahpur, A review on macro-level modeling of planar solid oxide fuel cells, *Int. J. Energy Res.*, **32**, 336-355, 2008

[5] D. Bhattacharyya and R. Rengaswamy, A review of solid oxide fuel cell (SOFC) dynamic models, *Ind. Eng. Chem. Res.*, **48**, 6068-6086, 2009

[6] K. Wang, D. Hissel, M.C. Pera, N. Steiner, D. Marra, M. Sorrentino, C. Pianese, M. Monteverde, P. Cardone and J. Saarinen, A Review on solid oxide fuel cells, *Int. J. Hydrogen Energy*, **36**, 7212-7228, 2011

[7] K. Wang, M.C. Péra, D. Hissel, N. Yousfi Steiner, A. Pohjoranta, S. Pofahl, SOFC modelling based on discrete Bayesian network for system diagnosis use, In proceedings of 8th IFAC Power Plant and Power System Control Symposium, 2.-5. September 2012, Toulouse (FR), 8(1), 675-680, 2012, DOI: 10.3182/20120902-4-FR-2032.00118

[8] M. Sorrentino, D. Marra, C. Pianese, M. Guida, F. Postiglione, K. Wang, A. Pohjoranta, On the Use of Neural Networks and Statistical Tools for Nonlinear Modeling and On-field Diagnosis of Solid Oxide Fuel Cell Stacks, *Energy Procedia*, **45**, 298-307, 2014

[9] M. Halinen, A. Pohjoranta, J. Pennanen, J. Kiviaho, Stack temperature estimation in system environment by utilizing the design of experiments methodology, *ECS Trans.*, **57** (1), 205-214, 2013

[10] H.-B. Huo, X.-J. Zhu, W.-Q. Hu, H.-Y. Tu, J. Li, J. Yang, Nonlinear model predictive control of SOFC based on a Hammerstein model, *J. Power Sources*, **185**(1), 338-344, 2008

[11] D.C. Montgomery, Design and Analysis of Experiments, 8th ed., John Wiley & Sons, 2009

[12] R.C. Dante, J.L. Escamilla, V. Madrigal, T. Theuss, J. de Dios Calderón, O. Solorza, R. Rivera, Fractional factorial design of experiments for PEM fuel cell performances improvement, *Int. J. Hydrogen Energy*, **28**(3), 343-348, 2003

[13] G.H. Guvelioglu, H.G. Stenge, Main and interaction effects of PEM fuel cell design parameters, *J. Power Sources*, **156**(2), 424-433, 2006

[14] B. Wahdame, D. Candusso, X. François, F. Harel, J.-M. Kauffmann, G. Coquery, Design of experiment techniques for fuel cell characterisation and development, *Int. J. Hydrogen Energy*, **34** (2), 967-980, 2009

[15] S. Endoo, K Pruksathorn, P. Piumsomboon, Identification of the key variables in membrane electrode preparation for PEM fuel cells by a factorial design, *Renewable Energy*, **35**(4), 807-813, 2010

[16] M. Calì, M.G.L. Santarelli, P. Leone, Design of experiments for fitting regression models on the tubular SOFC CHP 100 kW_e: Screening test, response surface analysis and optimization, *Int. J. Hydrogen Energy*, **32**(3), 343-358, 2007

[17] A. Esposito, P. Mocoteguy, F. Postiglione, M. Guida, C. Pianese, A. Pohjoranta, K. Wang, D. Hissel, M.C. Péra, S. Pofahl, Experimental test plan and data analysis based on the design of experiment methodology, *In Proceedings: ASME 2012 10th Int. Conf. Fuel Cell Sci. Eng. Tech.*, San Diego, Ca., USA, Jul. 23–26, 293-302, 2012

[18] A. Pohjoranta, M. Halinen, J. Pennanen, J. Kiviaho, Multivariable linear regression for SOFC stack temperature estimation under degradation effects, *J. Electrochemical Soc.*, **161**, F425-F433, 2014

[19] M. Halinen, A. Pohjoranta, J. Pennanen, J. Kiviaho, Application of Multivariable Regression Model for SOFC Stack Temperature Estimation in System Environment, accepted for publication in the 11th European SOFC and SOE Forum, Lucerne (CH), July 1.-4., 2014

[20] A. Pohjoranta, M. Halinen, J. Pennanen, J. Kiviaho, Dynamic SOFC Temperature Estimation with Designed Experiments and Time-Series Model Identification, accepted for publication in the 11th European SOFC and SOE Forum, Lucerne (CH), July 1.-4., 2014

[21] R.E. Kalman, A new approach to linear filtering and prediction problems, *Trans. ASME-J. Basic Eng.*, **82** (D), 35-45, 1960

[22] M. Halinen, M. Rautanen, J. Saarinen, J. Pennanen, A. Pohjoranta, J. Kiviaho, M. Pastula, B. Nuttall, C. Rankin and B. Borglum, Performance of a 10 kW SOFC Demonstration Unit Stacks and Systems, *ECS Trans.*, **35** (1), 113-120, 2011

[23] B. Borglum, E. Tang, M. Pastula, Development of solid oxide fuel cells at Versa Power Systems, *ECS Trans.*, **35** (1), 63-69, 2011

[24] L. Ljung, System identification - Theory for the user, 2nd ed., Prentice Hall PTR, 1999

[25] D. Simon, Optimal state estimation - Kalman, Hinf and Nonlinear Approaches, John Wiley & Sons, 2006